


Article

Biosynthesis of Schwertmannite and Goethite in a Bioreactor with Acidophilic Fe(II)-Oxidizing Betaproteobacterium Strain GJ-E10

Naoyuki Miyata ^{1,*} , Ayato Takahashi ¹, Tatsuo Fujii ², Hideki Hashimoto ³ and Jun Takada ^{2,4}

¹ Department of Biological Environment, Akita Prefectural University, Shimoshinjo-Nakano, Akita 010-0195, Japan; b11g021@yahoo.co.jp

² Graduate School of Natural Science and Technology, Okayama University, 3-1-1 Tsushimanaka, Okayama 700-8530, Japan; tfujii@cc.okayama-u.ac.jp (T.F.); jtakada@cc.okayama-u.ac.jp (J.T.)

³ Department of Applied Chemistry, School of Advanced Engineering, Kogakuin University, 2665-1 Nakano, Hachioji, Tokyo 192-0015, Japan; hideki-h@cc.kogakuin.ac.jp

⁴ Japan Science and Technology Agency (JST), Core Research for Evolutional Science and Technology (CREST), 3-1-1 Tsushimanaka, Okayama 700-8530, Japan

* Correspondence: nmiyata@akita-pu.ac.jp; Tel.: +81-18-872-1660

Received: 12 February 2018; Accepted: 1 March 2018; Published: 4 March 2018

Abstract: Iron oxide minerals, schwertmannite and goethite, which are naturally occurring in acidic environments are attractive nanostructured materials because of the potential diverse applications. Although the biosynthesis of schwertmannite by acidophilic Fe(II)-oxidizing microorganisms has been investigated, little is known about goethite biosynthesis under acidic conditions. To examine a biological approach to the synthesis of these minerals, bioreactor experiments were conducted with a newly isolated acidophilic betaproteobacterium. The bioproducts were characterized by powder X-ray diffraction, cryogenic Mössbauer spectroscopy, and electron microscopy. The cultures growing at 25 °C and pH 3.0 or at 37 °C and pH 2.5 oxidized Fe(II) and precipitated schwertmannite rapidly. Increasing pH at each temperature resulted in the concomitant production of goethite, and 90% pure goethite was obtained at 37 °C and pH 3.5. The goethite phase was nano-sized and had relatively large specific surface area ($133 \text{ m}^2 \cdot \text{g}^{-1}$), leading to high sorption capacity for metal oxyanions. Schwertmannite was also a good adsorbent for oxyanions, regardless of the smaller specific surface area. Our results indicate that these acidophilic microbial cultures serve as a simple rapid system for the synthesis of nanostructured goethite as well as schwertmannite.

Keywords: acidophilic iron-oxidizing bacterium; goethite; metal oxyanion sorption; Mössbauer spectroscopy; schwertmannite

1. Introduction

Schwertmannite $[\text{Fe}_8\text{O}_8(\text{OH})_{8-2x}(\text{SO}_4)_x]$; usually $1 \leq x \leq 1.75$ is a poorly crystallized iron hydroxide mineral occurring in sulfate-rich acidic environments (pH 2.5 to 4), including acid mine drainages, sulfuric acid soils, and acidic springs. Inorganic oxidation of Fe(II) by O_2 proceeds spontaneously, but is slow under these acidic conditions. Acidophilic Fe(II)-oxidizing microorganisms living in the environment catalyze Fe(II) oxidation to Fe(III). The Fe(III) ion is readily hydrolyzed and thus forms Fe(III) hydroxide minerals, so that the microbial activity is a crucial factor for controlling Fe(II) oxidation and mobility in the environment [1,2]. Goethite ($\alpha\text{-FeOOH}$) also occurs in the environment. Schwertmannite is metastable with goethite, and the transformation to goethite proceeds for weeks to months, depending on the conditions, including pH, temperature, ionic strength, and the presence of inorganic solutes [3–8]. The microbial metabolic activity causes facile transformation

to goethite, which proceeds for a few weeks during increasing pH and Fe(II) concentration in the surroundings of the schwertmannite phase [9].

Schwertmannite and goethite phases synthesized under laboratory conditions have received increasing attention with regard to environmental applications. The high sorption ability of schwertmannite for several oxyanions has been demonstrated, e.g., for As(V), As(III), Cr(VI), Mo(VI), and Se(VI) [10–14]. Arsenic(III) was reported to be effectively removed from artificial As-contaminated groundwater by schwertmannite, even in the presence of 750-fold higher molar concentrations of phosphate and sulfate [15]. The goethite phases are also an effective adsorbent of metal oxyanions, such as As(III/V), Se(IV/VI), and Cr(VI), and cations, such as Cu(II) and Cd(II) [16–18].

The biosynthesis of schwertmannite has been examined in laboratory cultures of an acidophilic Fe(II) oxidizing bacterium, *Acidithiobacillus ferrooxidans*. It utilizes Fe(II) as an energy source and grows autotrophically by CO₂ fixation, so that the schwertmannite production takes place in a simple mineral-salt medium at an ambient temperature. Although schwertmannite can be synthesized chemically via Fe(II) oxidation by H₂O₂ [4] or hydrolysis of Fe(III) [19], the biological method has proven to be a good alternative approach. Several studies have examined the effects of medium composition, pH, and temperature on the schwertmannite production by *A. ferrooxidans* [20–27]. In batch culture systems with a sulfate-rich medium, schwertmannite is formed under a wide range of conditions: e.g., at initial pH of 2.3–2.6, 36 °C, and NH₄⁺ concentrations of ~11 mM [20], and at pH of 1.6–3.4 and 26 °C [22]. In these studies, however, the medium pH has not been maintained at a constant level during the cultivation and decreased to 2 or less, even though it was initially set above 3. One study showed that medium pH strongly affects the mineral formation, in a jar fermenter system where initial pH was maintained [28]. Semiquantitative analysis based on dissolution in acidic ammonium oxalate revealed that schwertmannite is the only phase formed at pH 3.0 and 24 °C in *A. ferrooxidans* cultures. An increase in medium pH to 3.3 and 3.6 results in the formation of mixed phases of schwertmannite and goethite. Schwertmannite is still a major component (~58%); however, that study suggests that controlling culture conditions, such as pH and temperature, may enable rapid biosynthesis of goethite as a major component. Furthermore, only limited research has addressed acidophilic Fe(II) oxidizers other than *A. ferrooxidans*. The schwertmannite formation in cultures of *Ferroplasma myxofaciens* has been reported [29,30]. Given the varieties of acidophilic Fe(II)-oxidizing microorganisms and the potential applications, it is important to extend the range of available microbial strains and to characterize the Fe(II) oxidation kinetics and mineral formation.

The aim of this study was to demonstrate that schwertmannite and goethite are produced via the biological approach by a newly isolated acidophilic Fe(II)-oxidizing betaproteobacterium: strain GJ-E10 [31]. Batch culture experiments were conducted in a jar fermenter system to show the effect of medium pH and temperature on the Fe(II) oxidation kinetics and iron mineral formation. The kinetic data were used to indicate the biotic and abiotic contributions to the Fe(II) oxidation under different conditions. Quantitative and qualitative analyses, including powder X-ray diffraction (XRD), cryogenic Mössbauer spectroscopy, and electron microscopy, revealed the mineral forms of biogenic Fe precipitates in the cultures. Based on the nano-sized structures and large capacity values for adsorption of metal oxyanions, the biogenic iron minerals may serve as materials attractive for potential environmental technological applications.

2. Materials and Methods

2.1. The Microorganism and Culture Conditions

Bacterial strain GJ-E10 is an acidophilic Fe(II)-oxidizing chemolithoautotroph isolated from an acidic river environment in Akita, Japan [31]. The previously reported liquid medium [32] was modified and used in this study. It contained (per liter; pH 3.0) 1950 mg of FeSO₄·7H₂O, 1250 mg of (NH₄)₂SO₄, 500 mg of MgSO₄·7H₂O, 5 mg of K₂HPO₄, and 2 mL of a solution of trace mineral salts. The initial concentration of the Fe(II) ion was 390 mg·L⁻¹ (7 mM). A stock FeSO₄ solution prepared

with 25 mM sulfuric acid and a stock K_2HPO_4 solution was separately sterilized and added. The trace mineral-salt solution contained (per liter) 3.7 g of $CaCl_2 \cdot 2H_2O$, 2.5 g of H_3BO_3 , 0.87 g of $MnCl_2 \cdot 4H_2O$, 1.0 g of $FeCl_3 \cdot 6H_2O$, 0.44 g of $ZnSO_4 \cdot 7H_2O$, 0.29 g of $Na_2MoO_4 \cdot 2H_2O$, and 5 mg of $CuSO_4 \cdot 5H_2O$. The cultures were maintained in 100 mL conical flasks on a reciprocal shaker at 25 °C.

2.2. Bioreactor Experiments

The batch culture of strain GJ-E10 was conducted with a 5 L cylindrical jar fermenter system (Type TS-A5L; Takasugi MFG Co., Arakawa, Japan). In the culture medium, the concentration of $FeSO_4 \cdot 7H_2O$ was increased from 1950 to 7780 $mg \cdot L^{-1}$ (=28 mM). Sterile 4 L of the culture medium was aseptically inoculated with 80 mL of culture pregrown for 1 week, aerated at $2.0 L \cdot min^{-1}$ with filter-sterilized air, and was agitated moderately with a paddle impeller at a speed of 100 rpm. During the cultivation, the temperature was kept at 25 °C and pH was automatically maintained at 2.2 ± 0.1 , 2.5 ± 0.1 , 3.0 ± 0.1 , 3.5 ± 0.1 , 3.8 ± 0.1 , or 4.2 ± 0.1 with 1 M sodium hydroxide and 0.5 M sulfuric acid. Such cultures were also examined at 37 °C and pH 2.5 ± 0.1 , 3.0 ± 0.1 , and 3.5 ± 0.1 . The sampled culture fluid was centrifuged at $12,000 \times g$ for 10 min, and concentration of the Fe(II) ion in the supernatant was determined spectrophotometrically with 1,10-phenanthroline [33]. Time courses of residual Fe(II) in cultures were subjected to the kinetic analysis with Equation (1) [34], which is derived from the Monod equation. This logarithmic model assumes that the initial concentration of a growth substrate [28 mM Fe(II)] is much greater than the half-saturation constant for growth ($K_s \ll S_0$) [34]. Thus, the model could be applied to the data where enough substrate is still left in the culture.

$$S = S_0 + X_0[1 - \exp(\mu_{max} \cdot t)] \quad (1)$$

where S is the substrate concentration [Fe(II) ion; mM] at time point t (h), S_0 is the initial substrate concentration (mM), X_0 corresponds to the amount of substrate that is required to produce initial population density (mM), and μ_{max} is the maximum specific growth rate (h^{-1}). The kinetic parameters X_0 and μ_{max} were calculated via nonlinear regression in Prism 5.0 (GraphPad Software Inc., La Jolla, CA, USA). In this study, X_0 that was determined for the cultures at pH 3.0 served as a fixed value in the analysis of other pH conditions. For comparison, abiotic incubation without GJ-E10 cells was also examined under different pH and temperature conditions, and the Fe(II) concentration data monitored were analyzed by means of first-order kinetics (Equation (2)):

$$S = S_0 \cdot \exp(-k \cdot t) \quad (2)$$

where k is the first-order rate constant (h^{-1}).

2.3. Characterization of Iron Mineral Products

The products precipitated in the Fe(II)-oxidizing batch cultures were collected by centrifugation at $8000 \times g$ for 15 min, washed once with 0.5 mM sulfuric acid, and three times with Milli-Q water. For XRD analysis, the washed samples were air-dried and ground into a powder in a mortar. XRD measurements were carried out on a RINT-2500 diffractometer (Rigaku Co., The Woodlands, TX, USA) with CuK_{α} radiation at 20 mA and 40 kV. The crystallite sizes of goethite were estimated from the full-width at the half maximum of (101) diffraction peaks at 21.2° . XRD of well-crystallized Fe_2O_3 purchased from Wako Pure Chemicals was used to measure the instrumental broadening [$=0.182^\circ$ for (104) diffraction at 33.2°]. The calculation was conducted by means of the Scherrer Equation (Equation (3)).

$$D = 0.9\lambda(\beta \cdot \cos \theta)^{-1} \quad (3)$$

where D is the mean crystallite dimension, and λ and θ are the wavelength of X-ray radiation (CuK_{α} , 1.5406 Å) and Bragg angle, respectively; β is the full width at a half maximum, excluding the instrumental broadening.

Cryogenic Mössbauer measurements were performed at 100 K in transmission geometry using a conventional Mössbauer spectrometer with a 925 MBq $^{57}\text{Co}/\text{Rh}$ source. The velocity scale of Mössbauer spectra was calibrated with reference to α -iron. The washed then freeze-dried samples were subjected to transmission electron microscopy (TEM) under a JEM 1200EX (Jeol Co., Tokyo, Japan) at 80 kV. To show the capacity of oxyanion sorption, selected samples were also subjected to measurement of Brunauer-Emmett-Teller (BET)-specific surface area by N_2 absorption at 77 K. Total iron content of schwertmannite or goethite was determined spectrophotometrically with 1,10-phenanthroline after dissolution in hydrochloric acid.

2.4. Sorption Experiments with Metal Oxyanions

For examining the metal sorption by biogenic iron solids, the batch cultures were carried out at 25 °C and pH 3.0 for 74 h and at 37 °C and pH 3.5 for 41 h for the production of schwertmannite and goethite, respectively. The washed then freeze-dried solids were resuspended in Milli-Q water at 150 mg·L⁻¹, and a stock solution of sodium arsenate [As(V)], sodium arsenite [As(III)], sodium chromate [Cr(VI)], or sodium selenate [Se(VI)] was added to the suspensions at concentrations ranging from 5 to 100 mg·L⁻¹. These mixtures were shaken moderately at 25 °C until the aqueous-phase metal ions reached a steady state. During the incubation, the pH of the suspensions was periodically monitored and adjusted to 4 manually with H_2SO_4 or NaOH solution. Parallel control experiments were conducted with similar solutions without iron solids. Aqueous-phase metal ions in suspensions were quantified after centrifugation at 12,000 × g for 10 min on an X-series II inductively coupled plasma-mass spectrometer (ICP-MS; Thermo Fisher Scientific Inc., Waltham, MA, USA). The amount of metal adsorbed was calculated by subtracting the experimental aqueous-phase concentration from that of the corresponding control solution. The sorption isotherms obtained for the metal oxyanions were applied to the Langmuir equation to estimate the maximum metal sorption capacity in solids. The calculation was carried out in the Prism 5.0 software.

3. Results and Discussion

3.1. Fe(II) Oxidation Kinetics in Batch Cultures

In batch cultures grown at 25 °C in the pH range of 2.2 to 3.8, Fe(II) oxidation proceeded slowly during the first day and rapidly thereafter (Figure 1). In this study, it was assumed that under the substrate Fe(II)-rich conditions the Fe(II) oxidation rate increases with increasing the number of cells exponentially [34], so that the model Equation 1 was applied to data analysis. The result of the calculation showed good fitness to the data ($R^2 > 0.98$; Table S1, Supplementary Materials). Only limited rates of Fe(II) oxidation were obtained in a non-inoculated medium at 25 °C and pH 3.5 and 3.8 (Figure 1), and no oxidation was observed at pH < 3.0 within 72 h, indicating that the contribution of abiotic oxidation could be ruled out under these conditions. Based on the calculation, the periods of 4800 and 2900 h are needed for oxidation of 90% of the Fe(II) amount that was initially added to the cultures at pH 3.5 and 3.8, respectively, while only about 50 h is needed for biotic 90% oxidation (Table S2). At pH 4.2, however, Fe(II) oxidation by strain GJ-E10 strongly decreased, and the contribution of abiotic oxidation became significant. The data could not be fitted to Equation (1) (Figure 1). At pH 2.2 to 3.8, μ_{max} was dependent on medium pH and was the highest around pH 2.5 to 3.5 (Figure 2). Furthermore, the Fe(II) oxidation in cultures at pH > 2.5 resulted in the precipitation of yellowish brown iron hydroxides, whereas no iron solid was formed in the culture at pH 2.2, indicating fully dissolved Fe(III) ions.

Increasing the culture temperature to 37 °C resulted in an increase in the Fe(II) oxidation rate (Table S1 and Figure S1). Because abiotic oxidation in the non-inoculated medium was still minor in the pH range of 2.5 to 3.5 (Table S2), the increase in the oxidation rate likely resulted from the enhanced microbial growth. In that pH range, μ_{max} values were 1.6 to 1.8 times those that were obtained for cultures at 25 °C (Figure 2). These results indicated that the reaction catalyzed by GJ-E10 cells was fast

and contributed predominantly to the Fe(II) oxidation and precipitation of solids at least under the conditions excluding 25 °C and pH 4.2.

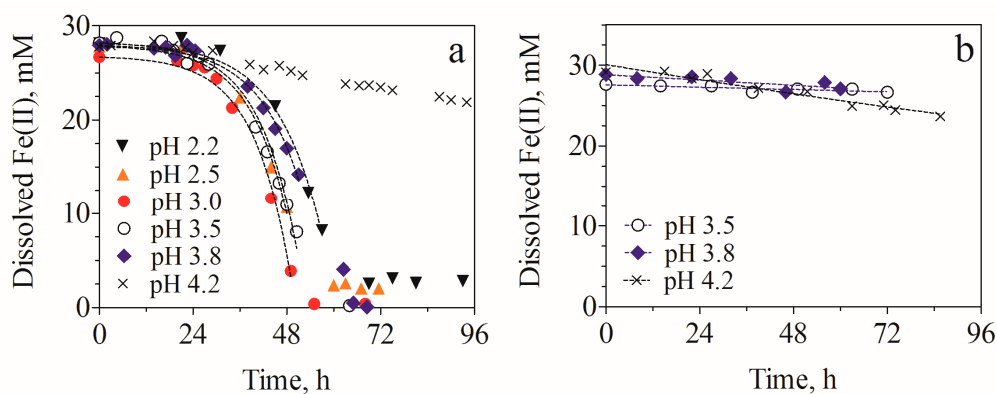


Figure 1. Fe(II) oxidation kinetics in cultures of strain GJ-E10 (a) and in an abiotic medium (b) under different pH conditions at 25 °C. The dashed lines show the nonlinear regression of the data to Equation (1), (a) and Equation (2), (b).

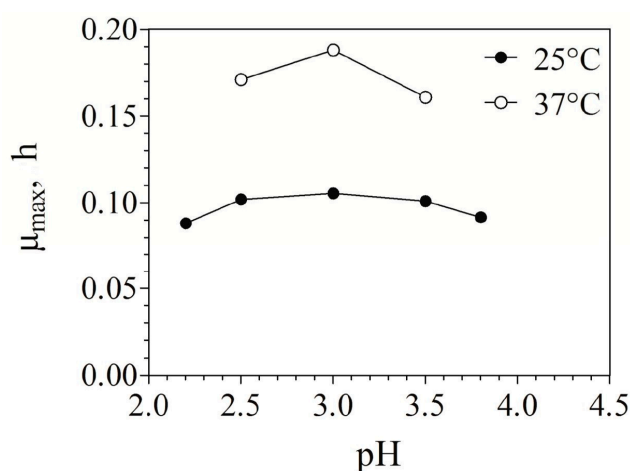


Figure 2. Effects of culture pH and temperature on the growth of strain GJ-E10.

3.2. Characteristics of Bioreactor Products

Bigham et al. [28] demonstrated the occurrence of mixed phases consisting of schwertmannite and goethite in acidic *A. ferrooxidans* cultures at 24 °C. Their culture grown at pH 3.0 yielded only a schwertmannite phase. In contrast, increasing the medium pH to 3.3 and 3.6 resulted in the concomitant formation of goethite, which was suggested to comprise ~12% and 42% of total solid iron, respectively, by semiquantitative analyses [28]. In the present study, our XRD (Figure 3) and Mössbauer spectroscopic data (Figure 4) were consistent with the previous report, and first indicated that these two phases were distinctively formed via control of the growth conditions of the acidophilic Fe(II) oxidizer. Although only schwertmannite formed in the cultures grown at 25 °C and pH 3.0, goethite phases appeared at pH 3.5 and 3.8 (Figure 3). Validity of these XRD patterns was confirmed in two or three independent bioreactor experiments. The formation ratio of schwertmannite to goethite could be evaluated quantitatively by Mössbauer spectroscopy (Figure 4 and Table 1). It is known that the Mössbauer spectrum of schwertmannite has a paramagnetic doublet pattern at temperatures down to 90 K [35], while the magnetic sextet pattern appears for goethite though the goethite nanoparticles show a superparamagnetic doublet pattern at room temperature [36]. The crystallite sizes of goethite

calculated from XRD peaks in Figure 3 were 10.3–22.7 nm (Table 1). To suppress the superparamagnetic behaviour of goethite nanoparticles, cryogenic Mössbauer measurements were performed at 100 K. Therefore, the relative area intensity of magnetic components in the Mössbauer spectra yielded the formation ratio of goethite, which accounted for 24% and 77% of total iron precipitates at pH 3.5 and 3.8 at 25 °C, respectively. The goethite formation was enhanced by increasing the culture temperature to 37 °C, and a 90% pure goethite phase was obtained at pH 3.5 (Figure 4). Again, under these conditions, the biological Fe(II) oxidation contributed mainly to the mineral formation. The TEM analysis revealed that the emergence of a goethite phase in the products resulted in the morphological change of whisker or filamentous structures typical for schwertmannite into very fine particulate forms with diameters of ~50 nm (Figure 5), consistent with the estimated crystallite size based on XRD. Similar structures of the mixed products in *A. ferrooxidans* cultures were reported [28]. The 90% pure goethite that was obtained at pH 3.5 and 37 °C had a BET-specific surface area of 133 m²·g^{−1}, while the schwertmannite phase at pH 3.0 and 25 °C showed 30 m²·g^{−1}.

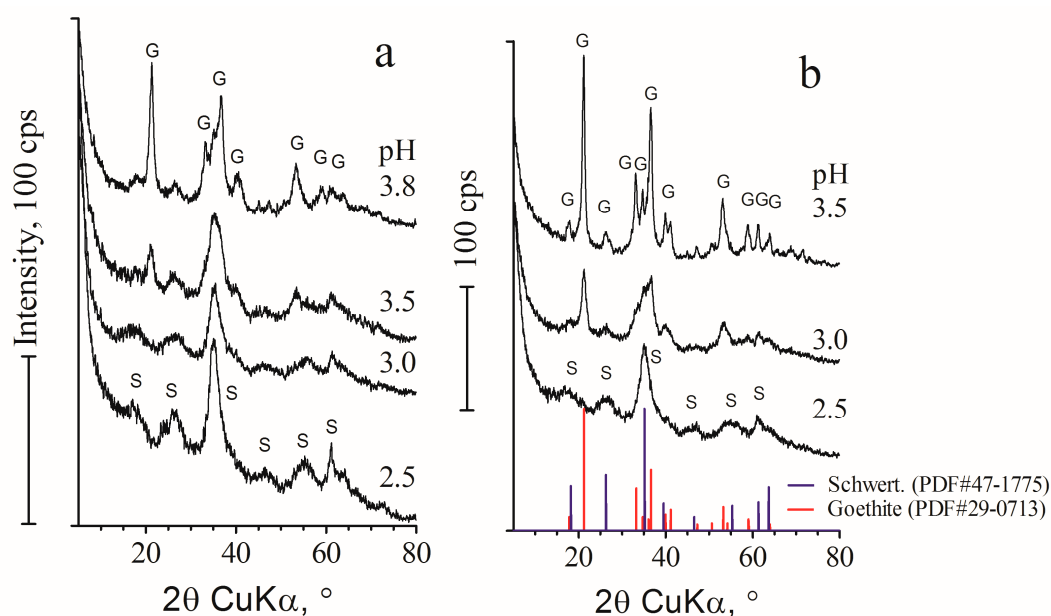


Figure 3. X-ray diffraction (XRD) patterns of biogenic iron oxide minerals formed in cultures at different pH levels at 25 °C (a) and 37 °C (b). ‘G’ and ‘S’ represent the diffraction of goethite and schwertmannite, respectively.

Table 1. Crystallite sizes of biogenic goethite estimated by the full-width at half-maximum XRD and the relative contents in solid iron estimated by cryogenic Mössbauer spectroscopy.

Culture Conditions	Full Width at Half Maximum (Degree) ¹	Crystallite Size (nm)	Relative Content in Solid Iron (%) ²
25 °C, pH 3.5	0.771	10.3	24
25 °C, pH 3.8	0.569	14.0	77
37 °C, pH 3.0	0.588	13.5	64
37 °C, pH 3.5	0.350	22.7	90.5

¹ Corrected values for (101) diffraction peaks at 21.2°. For XRD patterns, see Figure 3. ² For spectral data, see Figure 4.

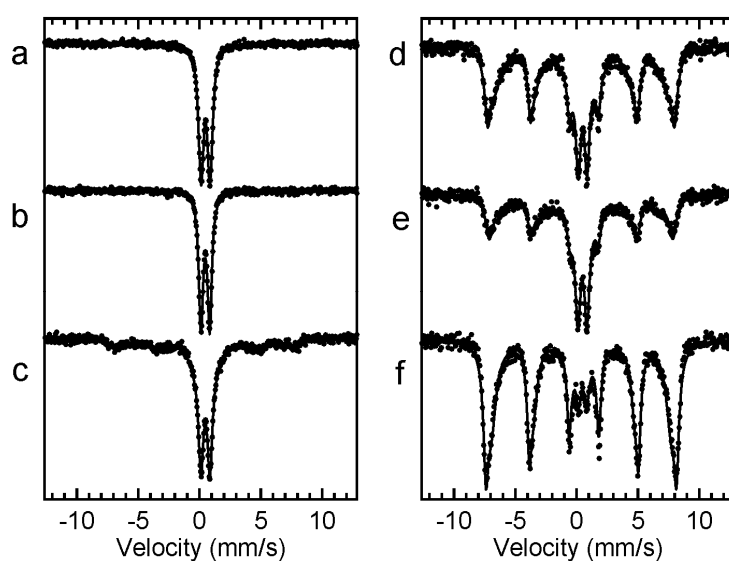


Figure 4. Cryogenic Mössbauer spectra at 100 K of biogenic iron oxide minerals formed in cultures at pH 2.5 (a); 3.0 (b); 3.5 (c); and 3.8 (d) at 25 °C and cultures at pH 3.0 (e) and 3.5 (f) at 37 °C. The spectra were fitted to a linear combination of normalized spectra (solid curves) of schwertmannite (sch) and goethite (goet): (a), 100% sch; (b), 100% sch; (c), 76% sch and 24% goet; (d), 23% sch and 77% goet; (e), 36% sch and 64% goet; (f), 9.5% sch and 90.5% goet.

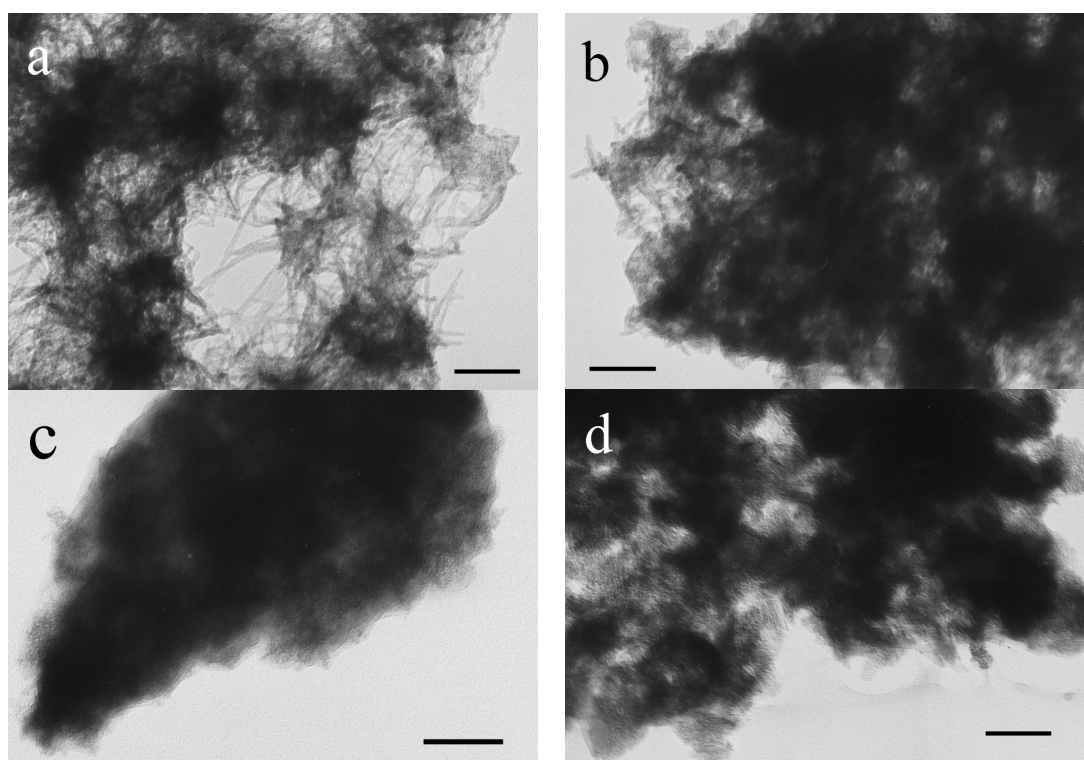


Figure 5. Transmission electron microscopy (TEM) images of biogenic iron oxide minerals formed in cultures at pH 3.0 (a); 3.5 (b); and 3.8 (c) at 25 °C and culture at pH 3.5 and 37 °C (d). Whisker structures typical for schwertmannite are major in panel a, while fine particulate forms representing the formation of goethite appear in panels b–d. Bar, 50 nm.

The previous study [28] and the present one clearly show that medium pH and temperature are the determinants of the biosynthesis of schwertmannite and goethite in acidophilic Fe(II)-oxidizing cultures. In addition, medium composition could greatly affect the mineral formation. Although only a schwertmannite phase formed at 25 °C and pH 2.5 in this study, such a low-pH medium was often reported to yield jarosite $[(\text{H},\text{Na},\text{K})\text{Fe}_3(\text{OH})_6(\text{SO}_4)_2]$ [20,23,28,29,37]. In this study, the concentration of NH_4^+ (=19 mM) appeared to be high enough to raise the jarosite formation [20,28]. The absence of emergence of jarosite in this study might have resulted from the short culture duration (41 or 74 h at pH 2.5). Many researchers adopted longer culture periods, which may allow for the phase transformation of schwertmannite to jarosite [20]. Extensive research has shown transformation of schwertmannite to goethite in the course of weeks to months in natural and artificial systems. The schwertmannite transformation is considered to be a major pathway for the formation of goethite phases in various environments. Based on the short-term bioreactor experiments (up to 120 h), Bigham et al. [28] suggested the direct precipitation of goethite as a product of Fe(III) hydrolysis. Our results support this claim and suggest that microbial Fe(II) oxidation can contribute significantly to the formation of goethite phases in acidic environments at relatively high temperature and pH.

3.3. Sorption of Metal Oxyanions to Bioreactor Products

The sorption isotherms of As(III), As(V), Cr(VI), and Se(VI) ions by the reactor products (Figure 6 and Table S3) revealed that the biogenic schwertmannite and goethite had large sorption capacity values for these metal oxyanions. Among the metals that were examined, schwertmannite adsorbed As(V) most effectively, and the amounts loaded reached $123 \text{ mg}\cdot\text{g}^{-1}$ (Table S3), which corresponded to the molar ratio of $225 \text{ mmol}_{\text{As}}\cdot\text{mol}_{\text{Fe}}^{-1}$. The sorption capacity values for As(III), Se(VI), and Cr(VI) were estimated as 128, 92, and $53 \text{ mmol}\cdot\text{mol}_{\text{Fe}}^{-1}$, respectively. Our data obtained with biogenic schwertmannite are comparable with the previous results, although experimental conditions somewhat differed from the previous studies [10,12,13], and this situation may yield the variation of sorption isotherms for the oxyanions. The schwertmannite preparations have As(V) sorption capacity of $>300 \text{ mmol}_{\text{As}}\cdot\text{mol}_{\text{Fe}}^{-1}$ for As(V) and $\sim 200 \text{ mmol}_{\text{As}}\cdot\text{mol}_{\text{Fe}}^{-1}$ for As(III) at pH 3.0 [10,12]. Lower sorption capacity was also shown for Cr(VI) ($90 \text{ mmol}_{\text{Cr}}\cdot\text{mol}_{\text{Fe}}^{-1}$) at pH 4.5 [13]. The As(V) sorption capacity obtained in this study is close to that of schwertmannite synthesized chemically ($190 \text{ mmol}_{\text{As}}\cdot\text{mol}_{\text{Fe}}^{-1}$ at pH 4.0) [13]. In spite of similar values for As(V) sorption, the values of specific surface area are largely different: $30 \text{ m}^2\cdot\text{g}^{-1}$ for biogenic schwertmannite vs. $171 \text{ m}^2\cdot\text{g}^{-1}$ for synthesized schwertmannite [13]. The sorption of metal oxyanions to schwertmannite involves the anion-exchange at surface sites, and the incorporation into schwertmannite (tunnel) structures [12,38]. The relatively small surface area in the biogenic product implies that the latter mechanism is more important for the As(V) sorption in schwertmannite [12]. The chemically synthesized schwertmannite with low specific surface area ($4\text{--}14 \text{ m}^2\cdot\text{g}^{-1}$) was reported to have the As(V) sorption capacity of $333 \text{ mmol}_{\text{As}}\cdot\text{mol}_{\text{Fe}}^{-1}$ at pH 3.0 [12].

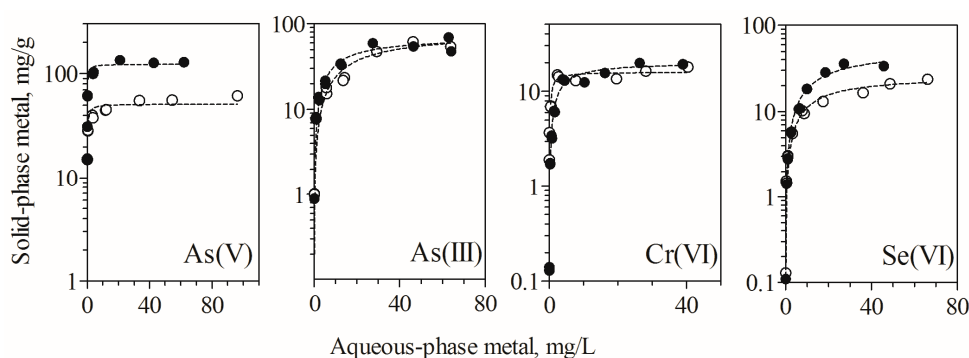


Figure 6. Sorption isotherms for As(V), As(III), Cr(VI), and Se(VI) oxyanions in biogenic schwertmannite and goethite. Filled and open circles represent the sorption by biogenic schwertmannite and goethite, respectively.

Our biogenic goethite adsorbed As(III) most effectively (Figure 6 and Table S3), and the maximum sorption capacity was estimated to be $126 \text{ mmol}_{\text{As}} \cdot \text{mol}_{\text{Fe}}^{-1}$ at pH 4. The sorption capacity values for As(V), Se(VI), and Cr(VI) were 79, 39, and 35 $\text{mmol} \cdot \text{mol}_{\text{Fe}}^{-1}$, respectively. It is most likely that the large capacity results from the high specific surface area. In goethite, the surface site where ligand exchange or complexation occurs is an important determinant of metal sorption capacity [18]. Although naturally occurring and synthetic goethite phases show a wide range of As(V) sorption capacity values per unit weight, they also show comparable capacity per unit surface area ($3\text{--}5 \text{ } \mu\text{mol} \cdot \text{m}^{-2}$) at pH 3–7 (Figure S2; data from Asta et al. [39]), indicating a higher sorption ability in the nano-sized particulate phase. The importance of the surface area for the sorption capacity of goethite preparations can also be demonstrated for Se(VI). The goethite preparation with low specific surface area ($2 \text{ m}^2 \cdot \text{g}^{-1}$) showed a maximum Se(VI) capacity of $1.1 \text{ } \mu\text{mol} \cdot \text{m}^{-2}$ [40], although the use of a high-ionic strength medium (0.1 M NaCl) may somewhat lower the sorption capability. Given the specific surface area ($133 \text{ m}^2 \cdot \text{g}^{-1}$) and the Se(VI) sorption capacity ($2.5 \text{ } \mu\text{mol} \cdot \text{m}^{-2}$), the biogenic goethite obtained in this study can adsorb a large amount of Se(VI) per unit weight.

Our data indicate that biogenic schwertmannite and goethite serve as good adsorbents for metal oxyanions. Research shows that owing to the low crystallinity or relatively high specific surface area, schwertmannite, and goethite nanoparticulates also serve as oxidative catalysts or oxidants for inorganic and organic contaminants (e.g., [41–45]). Another possible application includes the use of natural and synthetic goethite as an anodic material for microbial fuel cells [46]. Further work with the biogenic iron minerals should expand the range of environmental biotechnological application of acidophilic Fe(II)-oxidizing microorganisms.

4. Conclusions

In this study, we demonstrated that iron oxide minerals schwertmannite and goethite can be produced by an acidophilic Fe(II)-oxidizing bacterium in culture. The factors that significantly affect the mineral phase include culture pH and temperature. The biogenic schwertmannite and goethite serve as good adsorbents for metal oxyanions. In goethite, the nanostructural features leading to high specific surface area result in the high capacity for the sorption of metal oxyanions. This biological approach looks attractive because the mineral formation occurs under short-term simple bioreactor conditions.

Supplementary Materials: The following are available online at www.mdpi.com/2075-163X/8/3/98/s1, Figure S1: Fe(II) oxidation kinetics in cultures of strain GJ-E10 and in an abiotic medium at different pH levels at 37 °C, Figure S2: the relation between As(V) sorption capacity and specific surface area in goethite phases, Table S1: kinetics of biotic and abiotic Fe(II) oxidation at different temperatures and pH levels, Table S2: a comparison of biotic and abiotic oxidation of Fe(II) under different pH and temperature conditions, Table S3: sorption capacity values of metal oxyanions in schwertmannite and goethite phases formed in cultures of strain GJ-E10.

Acknowledgments: The authors thank T. Yamada, C. Sakamoto, and A. Ohishi for their work on microbial cultivation and characterization and on oxyanion sorption. This study was supported by JSPS KAKENHI Grant Numbers JP23510104 and JP26289261.

Author Contributions: N.M., T.F. and J.T. conceived and designed the experiments; N.M., A.T., T.F. and H.H. performed the experiments; N.M., T.F., H.H. and J.T. analyzed the data; and N.M. and T.F. wrote the paper.

Conflicts of Interest: The authors declare no conflict of interest.

References

1. Kawano, M.; Tomita, K. Geochemical modeling of bacterially induced mineralization of schwertmannite and jarosite in sulfuric acid spring water. *Am. Mineral.* **2001**, *86*, 1156–1165. [CrossRef]
2. Hedrich, S.; Schlömann, M.; Johnson, D.B. The iron-oxidizing proteobacteria. *Microbiology* **2011**, *157*, 1551–1564. [CrossRef] [PubMed]
3. Bigham, J.M.; Schwertmann, U.; Traina, S.J.; Winland, R.L.; Wolf, M. Schwertmannite and the chemical modeling of iron in acid sulfate waters. *Geochim. Cosmochim. Acta* **1996**, *60*, 2111–2121. [CrossRef]
4. Regenspurg, S.; Brand, A.; Peiffer, S. Formation and stability of schwertmannite in acidic mining lakes. *Geochim. Cosmochim. Acta* **2004**, *68*, 1185–1197. [CrossRef]

5. Schwertmann, U.; Carlson, L. The pH-dependent transformation of schwertmannite to goethite at 25 °C. *Clay Miner.* **2005**, *40*, 63–66. [[CrossRef](#)]
6. Knorr, K.-H.; Blodau, C. Controls on schwertmannite transformation rates and products. *Appl. Geochem.* **2007**, *22*, 2006–2015. [[CrossRef](#)]
7. Burton, E.D.; Johnston, S.G. Impact of silica on the reductive transformation of schwertmannite and the mobilization of arsenic. *Geochim. Cosmochim. Acta* **2012**, *96*, 134–153. [[CrossRef](#)]
8. Schoepfer, V.A.; Burton, E.D.; Johnston, S.G.; Kraal, P. Phosphate-imposed constraints on schwertmannite stability under reducing conditions. *Environ. Sci. Technol.* **2017**, *51*, 9739–9746. [[CrossRef](#)] [[PubMed](#)]
9. Bertel, D.; Peck, J.; Quick, T.J.; Senko, J.M. Iron transformation induced by an acid-tolerant *Desulfosporosinus* species. *Appl. Environ. Microbiol.* **2012**, *78*, 81–88. [[CrossRef](#)] [[PubMed](#)]
10. Carlson, L.; Bigham, J.M.; Schwetmann, U.; Kyek, A.; Wagner, F. Scavenging of As from acid mine drainage by schwertmannite and ferrihydrite: A comparison with synthetic analogues. *Environ. Sci. Technol.* **2002**, *36*, 1712–1719. [[CrossRef](#)] [[PubMed](#)]
11. Fukushi, K.; Sato, T.; Yanase, N. Solid-solution reactions in As(V) sorption by schwertmannite. *Environ. Sci. Technol.* **2003**, *37*, 3581–3586. [[CrossRef](#)] [[PubMed](#)]
12. Burton, E.D.; Bush, R.T.; Johnston, S.G.; Watling, K.M.; Hocking, R.K.; Sullivan, L.A.; Parker, G.K. Sorption of arsenic(V) and arsenic(III) to schwertmannite. *Environ. Sci. Technol.* **2009**, *43*, 9202–9207. [[CrossRef](#)] [[PubMed](#)]
13. Antelo, J.; Fiol, S.; Gondar, D.; López, R.; Arce, F. Comparison of arsenate, chromate and molybdate binding on schwertmannite: Surface adsorption vs. anion-exchange. *J. Colloid Interface Sci.* **2012**, *386*, 338–343. [[CrossRef](#)] [[PubMed](#)]
14. Song, J.; Jia, S.-Y.; Ren, H.-T.; Wu, S.-H.; Han, X. Application of high-surface-area schwertmannite in the removal of arsenate and arsenite. *Int. J. Environ. Sci. Technol.* **2015**, *12*, 1559–1568. [[CrossRef](#)]
15. Liao, Y.; Liang, J.; Zhou, L. Adsorptive removal of As(III) by biogenic schwertmannite from simulated As-contaminated groundwater. *Chemosphere* **2011**, *83*, 295–301. [[CrossRef](#)] [[PubMed](#)]
16. Hua, M.; Zhang, S.; Pan, B.; Zhang, W.; Lv, L.; Zhang, Q. Heavy metal removal from water/wastewater by nanosized metal oxides: A review. *J. Hazard. Mater.* **2012**, *211–212*, 317–331. [[CrossRef](#)] [[PubMed](#)]
17. Jaiswal, A.; Banerjee, S.; Mani, R.; Chattopadhyaya, M.C. Synthesis, characterization and application of goethite mineral as an adsorbent. *J. Environ. Chem. Eng.* **2013**, *1*, 281–289. [[CrossRef](#)]
18. Liu, H.; Chen, T.; Frost, R.L. An overview of the role of goethite surfaces in the environment. *Chemosphere* **2014**, *103*, 1–11. [[CrossRef](#)] [[PubMed](#)]
19. Loan, M.; Cowley, J.M.; Hart, R.; Parkinson, G.M. Evidence on the structure of synthetic schwertmannite. *Am. Mineral.* **2004**, *89*, 1735–1742. [[CrossRef](#)]
20. Wang, H.; Bigham, J.M.; Tuovinen, O.H. Formation of schwertmannite and its transformation to jarosite in the presence of acidophilic iron-oxidizing microorganisms. *Mater. Sci. Eng. C* **2006**, *26*, 588–592. [[CrossRef](#)]
21. Xiong, H.; Liao, Y.; Zhou, L. Influence of chloride and sulfate on formation of akaganéite and schwertmannite through ferrous biooxidation by *Acidithiobacillus ferrooxidans* cells. *Environ. Sci. Technol.* **2008**, *42*, 8681–8686. [[CrossRef](#)] [[PubMed](#)]
22. Liao, Y.; Zhou, L.; Liang, J.; Xiong, H. Biosynthesis of schwertmannite by *Acidithiobacillus ferrooxidans* cell suspensions under different pH condition. *Mater. Sci. Eng. C* **2009**, *29*, 211–215. [[CrossRef](#)]
23. Zhu, J.; Gan, M.; Zhang, D.; Hu, Y.; Chai, L. The nature of schwertmannite and jarosite mediated by two strains of *Acidithiobacillus ferrooxidans* with different ferrous oxidation ability. *Mater. Sci. Eng. C* **2013**, *33*, 2679–2685. [[CrossRef](#)] [[PubMed](#)]
24. Gan, M.; Zheng, Z.; Sun, S.; Zhu, J.; Liu, X. The influence of aluminum chloride on biosynthetic schwertmannite and Cu(II)/Cr(VI) adsorption. *RSC Adv.* **2015**, *5*, 94500–94512. [[CrossRef](#)]
25. Chai, L.; Tang, J.; Liao, Y.; Yang, Z.; Liang, L.; Li, Q.; Wang, H.; Yang, W. Biosynthesis of schwertmannite by *Acidithiobacillus ferrooxidans* and its application in arsenic immobilization in the contaminated soil. *J. Soils Sediments* **2016**, *16*, 2430–2438. [[CrossRef](#)]
26. Mukherjee, C.; Jones, F.S.; Bigham, J.M.; Tuovinen, O.H. Synthesis of argentojarosite with simulated bioleaching solutions produced by *Acidithiobacillus ferrooxidans*. *Mater. Sci. Eng. C* **2016**, *66*, 164–169. [[CrossRef](#)] [[PubMed](#)]

27. Zhang, J.; Shi, J.; Zhang, S.; Zhou, L.; Xu, J.; Ge, Y.; Fan, W.; Liu, F. Schwertmannite adherence to the reactor wall during the bio-synthesis process and deterioration of its structural characteristics and arsenic(III) removal efficiency. *Minerals* **2017**, *7*, 64. [\[CrossRef\]](#)
28. Bigham, J.M.; Schwertmann, U.; Pfab, G. Influence of pH on mineral speciation in a bioreactor simulating acid mine drainage. *Appl. Geochem.* **1996**, *11*, 845–849. [\[CrossRef\]](#)
29. Hedrich, S.; Lünsdorf, H.; Kleeberg, R.; Heide, G.; Seifert, J.; Schlömann, M. Schwertmannite formation adjacent to bacterial cells in a mine water treatment plant and in pure cultures of *Ferroplasma myxofaciens*. *Environ. Sci. Technol.* **2011**, *45*, 7685–7692. [\[CrossRef\]](#) [\[PubMed\]](#)
30. Hedrich, S.; Johnson, D.B. A modular continuous flow reactor system for the selective bio-oxidation of iron and precipitation of schwertmannite from mine-impacted waters. *Bioresour. Technol.* **2012**, *106*, 44–49. [\[CrossRef\]](#) [\[PubMed\]](#)
31. Fukushima, J.; Tojo, F.; Asano, R.; Kobayashi, Y.; Shimura, Y.; Okano, K.; Miyata, N. Complete genome sequence of the unclassified iron-oxidizing, chemolithoautotrophic *Burkholderiales* bacterium GJ-E10, isolated from an acidic river. *Genome Announc.* **2015**, *3*, e01455-14. [\[CrossRef\]](#) [\[PubMed\]](#)
32. Bryan, C.G.; Johnson, D.B. Dissimilatory ferrous iron oxidation at a low pH: A novel trait identified in the bacterial subclass *Rubrobacteridae*. *FEMS Microbiol. Lett.* **2008**, *288*, 149–155. [\[CrossRef\]](#) [\[PubMed\]](#)
33. Japan Sewage Works Association. *Sewage Analytical Methods*; Japan Sewage Works Association: Tokyo, Japan, 1997; pp. 271–274.
34. Simkins, S.; Alexander, M. Models for mineralization kinetics with the variables of substrate concentration and population density. *Appl. Environ. Microbiol.* **1984**, *47*, 1299–1306. [\[PubMed\]](#)
35. Bigham, J.M.; Carlson, L.; Murad, E. Schwertmannite, a new iron oxyhydroxysulphate from Pyhäsalmi, Finland, and other localities. *Mineral. Mag.* **1994**, *58*, 641–648. [\[CrossRef\]](#)
36. Frandsen, C.; Madsen, D.E.; Boothroyd, C.B.; Mørup, S. Anomalous particle size dependence of magnetic relaxation phenomena in goethite nanoparticles. *Croat. Chem. Acta* **2015**, *88*, 481–485. [\[CrossRef\]](#)
37. Gan, M.; Song, Z.; Jie, S.; Zhu, J.; Zhu, Y.; Liu, X. Biosynthesis of bifunctional iron oxyhydroxysulfate by *Acidithiobacillus ferrooxidans* and their application to coagulation and adsorption. *Mater. Sci. Eng. C* **2016**, *59*, 990–997. [\[CrossRef\]](#) [\[PubMed\]](#)
38. Fukushi, K.; Sato, T.; Yanase, N.; Minato, J.; Yamada, H. Arsenate sorption on schwertmannite. *Am. Mineral.* **2004**, *89*, 1728–1734. [\[CrossRef\]](#)
39. Asta, M.P.; Cama, J.; Martínez, M.; Giménez, J. Arsenic removal by goethite and jarosite in acidic conditions and its environmental implications. *J. Hazard. Mater.* **2009**, *171*, 956–972. [\[CrossRef\]](#) [\[PubMed\]](#)
40. Rovira, M.; Giménez, J.; Martínez, M.; Martínez-Lladó, X.; De Pablo, J.; Martí, V.; Duro, L. Sorption of selenium(IV) and selenium(VI) onto natural iron oxides: Goethite and hematite. *J. Hazard. Mater.* **2008**, *150*, 279–284. [\[CrossRef\]](#) [\[PubMed\]](#)
41. Lin, K.; Ding, J.; Wang, H.; Huang, X.; Gan, J. Goethite-mediated transformation of bisphenol A. *Chemosphere* **2012**, *89*, 789–795. [\[CrossRef\]](#) [\[PubMed\]](#)
42. Wang, W.-M.; Song, J.; Han, X. Schwertmannite as a new Fenton-like catalyst in the oxidation of phenol by H₂O₂. *J. Hazard. Mater.* **2013**, *262*, 412–419. [\[CrossRef\]](#) [\[PubMed\]](#)
43. Yang, G.C.C.; Huang, S.-C.; Wang, C.-L.; Jen, Y.-S. Degradation of phthalate esters and acetaminophen in river sediments using the electrokinetic process integrated with a novel Fenton-like process catalyzed by nanoscale schwertmannite. *Chemosphere* **2016**, *159*, 282–292. [\[CrossRef\]](#) [\[PubMed\]](#)
44. Meng, X.; Yan, S.; Wu, W.; Zheng, G.; Zhou, L. Heterogeneous Fenton-like degradation of phenanthrene catalyzed by schwertmannite biosynthesized using *Acidithiobacillus ferrooxidans*. *RSC Adv.* **2017**, *7*, 21638–21648. [\[CrossRef\]](#)
45. Li, X.; Zhang, Y.; Xie, Y.; Zeng, Y.; Li, P.; Xie, T.; Wang, Y. Ultrasonic-enhanced Fenton-like degradation of bisphenol A using a bio-synthesized schwertmannite catalyst. *J. Hazard. Mater.* **2018**, *344*, 689–697. [\[CrossRef\]](#) [\[PubMed\]](#)
46. Peng, X.; Yu, H.; Wang, X.; Gao, N.; Geng, L.; Ai, L. Enhanced anode performance of microbial fuel cells by adding nanosemiconductor goethite. *J. Power Sources* **2013**, *223*, 94–99. [\[CrossRef\]](#)

